Research Paper

A shift in redox conditions near the Ediacaran/Cambrian transition and its possible influence on early animal evolution, Corumbá Group, Brazil

Fabricio A. Caxito [a,b,*], Erik Sperling [b], Gabriella Fazio [c], Rodrigo Rodrigues Adorno [d], Matheus Denezine [c], Dermeval Aparecido Do Carmo [c], Martino Giorgioni [c], Gabriel J. Uhlein [a], Alcides N. Sial [e]

[a] CPMTC Research Center and Programa de Pós-graduação em Geologia, Departamento de Geologia, Instituto de Geociências, Universidade Federal de Minas Gerais, Belo Horizonte, MG 31270-901, Brazil
[b] Department of Earth and Planetary Sciences, Doerr School of Sustainability, Stanford University, CA 94305, USA
[c] Instituto de Geociências, Universidade de Brasília, Brasília, DF 70910-900, Brazil
[d] Center for Applied Geosciences (CGA) of the Geological Survey of Brazil (SBG/CPRM), Brasília, Distrito Federal 70040-904, Brazil
[e] NEG LABISE, Universidade Federal de Pernambuco, Recife - PE 50740-530, Brazil

A B S T R A C T

The Ediacaran–Cambrian transition witnessed some of the most important biological, tectonic, climatic and geochemical changes in Earth's history. Of utmost importance for early animal evolution is the likely shift in redox conditions of bottom waters, which might have taken place in distinct pulses during the late Ediacaran and early Paleozoic. To track redox changes during this transition, we present new trace element, total organic carbon and both inorganic and organic carbon isotopes, and the first iron speciation data on the Tamengo and Guaicurus formations of the Corumbá Group in western Brazil, which record important paleobiological changes between 555 Ma to < 541 Ma. The stratigraphically older Tamengo Formation is composed mainly of limestone with interbedded marls and mudrocks, and bears fragments of upper Ediacaran biomineralized fossils such as *Cloudina lucianoi* and *Corumbella werneri*. The younger Guaicurus Formation represents a regional transgression of the shallow carbonate platform and is composed of a homogeneous fine-grained siliciclastic succession, bearing meiofaunal bilateral burrows. The new iron speciation data reveal predominantly anoxic and ferruginous (non-sulfidic) bottom water conditions during deposition of the Tamengo Formation, with Fe_{HR}/Fe_T around 0.8 and Fe_{Py}/Fe_{HR} below 0.7. The transition from the Tamengo to the Guaicurus Formation is marked by a stratigraphically rapid drop in Fe_{HR}/Fe_T to below 0.2, recording a shift to likely oxic bottom waters, which persist upsection. Redox-sensitive element (RSE) concentrations are muted in both formations, but consistent with non-sulfidic bottom water conditions throughout. We interpret the collected data to reflect a transition between two distinct paleoenvironmental settings. The Tamengo Formation represents an environment with anoxic bottom waters, with fragments of biomineralized organisms that lived on shallower, probably mildly oxygenated surficial waters, and that were then transported down-slope. Similar to coeval successions (e.g., the Nama Group in Namibia), our data support the hypothesis that late Ediacaran biomineralized organisms lived in a thin oxygenated surface layer above a relatively shallow chemocline. The Guaicurus Formation, on the other hand, records the expansion of oxic conditions to deeper waters during a sea level rise. Although the relationship between global biogeochemical changes and the activities of early bioturbators remains complex, these results demonstrate an unequivocal synchronous relationship between oxygenation of the Corumbá basin and the local appearance of meiofaunal bioturbators.

1. Introduction

Reconstructing past oceanic and atmospheric redox conditions is essential to unravel possible feedback mechanisms between the chemical and biological evolution of planet Earth, especially for periods of important biological innovation. When coupled to

* Corresponding author.
    E-mail address: caxito@ufmg.br (F.A. Caxito).

paleontological and sedimentological data in stratigraphic sections, geochemical proxies for paleoredox conditions can potentially provide crucial information on how the biosphere responded to periods of major paleoenvironmental change and vice-versa.

The Proterozoic–Phanerozoic transition is recognized as one of the most extreme periods of coupled lithosphere-atmosphere-biosphere variation in the geological record, registering major plate tectonics reorganizations (Merdith et al., 2017), extreme climatic fluctuations (Hoffman et al., 2017), the initial diversification of animals and complex ecological behaviors (Xiao and Laflamme, 2009; Erwin et al., 2011; Wood et al., 2019; Bowyer et al., 2022), and a potential, albeit probably protracted, rise in atmospheric oxygen (Shields-Zhou and Och, 2011; Och and Shields-Zhou, 2012; Cole et al., 2020). Links between all of these processes are widely assumed (although still requiring considerable validation), and changes in seafloor redox conditions are commonly considered as potential key influences on early animal diversification (e.g., Mills and Canfield, 2014; Cole et al., 2020). Although the exact evolutionary mechanism(s) by which oxygen influenced animal evolution are unclear, it was most probably through crossing of critical ecological thresholds at low O_2 (Sperling et al., 2013, 2022) and through stabilization of metazoan extinction rates after O_2 rose to near-modern levels during the early Phanerozoic (Saltzman et al., 2015; Stockey et al., 2021).

A growing, multi-proxy body of analysis of Neoproterozoic to early Cambrian basins around the world has progressively replaced early views of a monotonic rise in atmospheric oxygen levels during this time frame towards a more nuanced and dynamic view, with protracted and heterogeneous oxygenation (and deoxygenation) of the marine realm spanning through the early Phanerozoic (Shields-Zhou and Och, 2011; Och and Shields-Zhou, 2012; Sperling et al., 2015; Wood et al., 2015; Bowyer et al., 2017; Dahl et al., 2017; Jin et al., 2018; He et al., 2019; Wei et al., 2018; Tostevin and Mills, 2020). In order to understand and further quantify the influence of rising oxygen levels in the early evolution and diversification of complex organisms that took place in this complex redox landscape, detailed chemostratigraphic reconstructions of key sedimentary basins that yield fossil remnants of these organisms is demanded.

Amongst the myriad techniques currently used for tracking ancient oceanic and atmospheric redox conditions, iron-based proxies are normally considered as one of the most effective and reliable tools, especially through the iron speciation technique, i.e., the quantification of the iron contents in distinct phase pools that are highly reactive (Fe_{HR}) towards sulfide on early diagenetic timescales (Poulton and Canfield, 2005, 2011; Lyons and Severmann, 2006; Raiswell et al., 2018; Bowyer et al., 2020). Although originally developed for fine-grained siliciclastic rocks, further work demonstrated the viability of the iron speciation proxy for other rock types such as carbonates, provided they yield sufficient total iron contents to buffer post-depositional enrichments in Fe, such as those caused by late-stage deep burial dolomitization (Clarkson et al., 2014). The arbitrary cut-off is normally set at around 0.5 wt.% Fe (Clarkson et al., 2014), but in practice, the reliability of iron speciation data to reflect redox trends of the original bottom waters can be assessed by the concordance of the proxy when applied to distinct rock types in the same section, e.g., siliciclastic horizons interbedded or associated with carbonate rocks in the same depositional cycle, and by the concordance of the acquired dataset with interpretations drawn by the use of other redox proxies in the same section (e.g. Tostevin et al., 2016).

Here, we present the first iron speciation data, along with novel trace element measurements, total organic carbon (TOC) contents and both inorganic and organic carbon isotopes, of mudstone, marl and carbonate samples of the Corumbá Group (Almeida, 1965) in

western Brazil (Figs. 1 and 2). The two uppermost units of this group, the Tamengo and Guaicurus formations, contain fragments of late Ediacaran index biomineralizing fossils such as *Cloudina lucianoi* (Beurlen and Sommer, 1957) and *Corumbella werneri* (Hahn et al., 1982) and meiofaunal bilaterian burrows (Parry et al., 2017). All this evidence indicates a complex ecological behavior throughout this section, which spans one of the most important intervals of biological innovation, the Ediacaran/Cambrian transition. The goal is to contribute to the ongoing debate on the influence of oxygen availability and biogeochemical conditions on the paleoenvironmental settings that allowed for the initial diversification of complex life forms during this key time frame in Earth's story.

2. Geological context

The Paraguay Belt is a curvilinear fold-and-thrust belt related to the Brasiliano Orogeny in western Brazil (Fig. 1), composed of Neoproterozoic to Cambrian metasedimentary and volcanoclastic units deposited in the southern and eastern margins of the Amazon Craton and Rio Apa block, respectively, that were deformed and metamorphosed during the amalgamation of western Gondwana, ca. 540 Ma (Tohver et al., 2010; McGee et al., 2012). The Paraguay Belt is usually subdivided into a northern, N/NW-verging sigmoidal segment bordering the southern margin of the Amazon Craton and a southern, W-verging segment bordering the eastern margin of the Rio Apa block, with the Corumbá graben system at the central portion linking those two fold belt arms and the WNW-trending Tucavaca Aulacogen that separates the Amazon Craton and Rio Apa block to the west, in Bolivia (Jones, 1985; Trompette et al., 1998; Walde et al., 2015). The Corumbá graben system is dominated by high-angle normal faults trending dominantly NE–SW and is filled by the Corumbá Group.

The Corumbá Group (Almeida, 1965; Boggiani, 1998) comprises, from bottom to top, the Cadieus, Cerradinho, Bocaina, Tamengo and Guaicurus formations. The first two units are dominated by detrital sedimentation with conglomerates, arkoses and shales, representing *syn*-rift sedimentation, while the post-rift Bocaina Formation comprises stromatolitic dolomites and phosphorites. The Tamengo and Guaicurus formations are studied in the present work and will be further detailed.

The Tamengo Formation comprises, from bottom to top, breccias and dolomites followed by thick dark gray limestones with interbedded mudrocks (Boggiani, 1998). Boggiani (1998) interpreted the Tamengo Formation as representing, at the breccia-dominated base of the succession, turbiditic sedimentation in a reworked slope, with progressively higher sea level towards the top of the unit, dominated by shelf carbonates and mudstones. According to Boggiani et al. (2010) and Fernandes et al. (2022) the basal breccias of the Tamengo Formation record an uplift cycle, resulting in the expression of regional drop in base level and causing the erosion of the carbonates found below, in the Bocaina Formation. The basal breccia and the lower part of the unit is marked by negatively fractionated $\delta^{13}C$ values (ca. $-3‰$; Boggiani et al., 2010). The shelf carbonates marking a transgressive event upsection record a positive $\delta^{13}C$ excursion (up to $+5‰$) (Boggiani et al., 2010; Spangenberg et al., 2014; Ramos et al., 2022). *Cloudina lucianoi* (Beurlen and Sommer, 1957) shells are found in the latter limestones, and *Corumbella werneri* (Hahn et al., 1982) occur in the associated mudrocks (Almeida, 1965; Zaine, 1991; Boggiani, 1998; Gaucher et al., 2003; Boggiani et al., 2010).

In the studied Laginha quarry (Fig. 2), the Tamengo Formation is composed, at the base, of ca. 20-m thick interval of carbonate breccia followed by ca. 8 m of dolostone layers, which in turn is capped by ca. 30 m of rhythmic facies including dark grainstone layers,
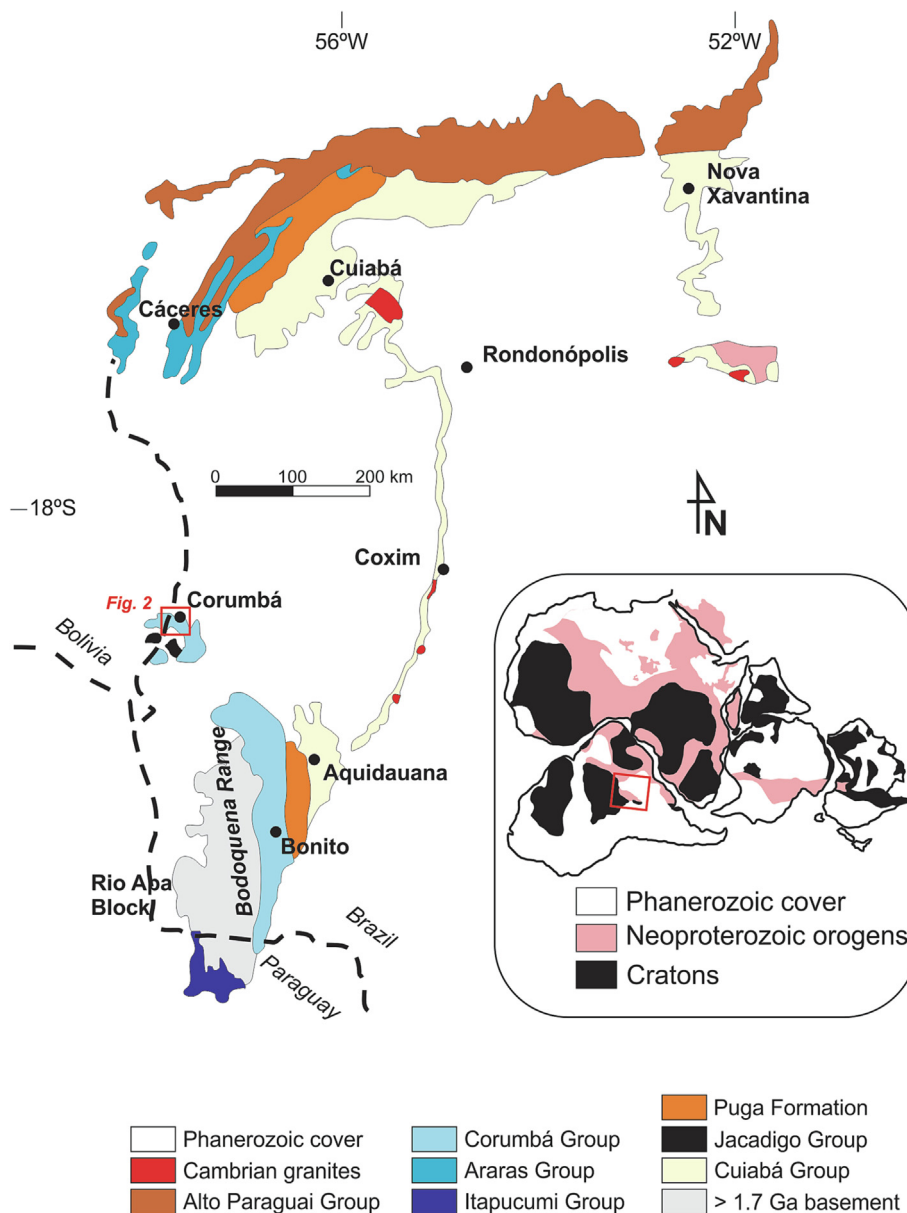
Fig. 1. Schematic geology of the Paraguay Belt in western Brazil. The inset at the bottom right shows the approximate position in western Gondwana. The studied area is marked in the red rectangle. Modified after Caxito et al. (2019). (For interpretation of the references to colour in this figure legend, the reader is referred to the web version of this article.)

locally with *Cloudina* fragments, interleaved with laminated mudrocks (mudstones, marls and lime mudstones). The contact between the Tamengo and Guaicurus Formations, at ca. 60 m in the section, is interpreted as abrupt (Adorno et al., 2017), but in other places it has been interpreted as transitional with interbedding of mudstones toward the top of the carbonate-dominated succession of the Tamengo Formation (Campanha et al., 2011).

The fossil occurrences of *Cloudina* and *Corumbella* in the Tamengo Formation are essentially allochtonous, with variably fragmented and fractured specimens, sometimes concentrated in single horizons, with clear signs of reworking and deposition along with fine-grained siliciclastics and carbonates (Pacheco et al., 2015; Amorim et al., 2020). Although Amorim et al. (2020) recognized the good preservation of the thin and delicate *Corumbella* walls in some specimens as possible indicators of little to no reworking, the authors also present an alternative explanation of deposition in predominantly low-energy settings. Thus, no defini-

tive arguments were presented for the occurrence of parautochthonous *Cloudina* or *Corumbella* in the Tamengo Formation.

The Guaicurus Formation consists of homogeneous silt/mudstone with plane-parallel lamination defined by the alternation of lighter and darker silt/mud laminae, deposited offshore, below the storm wave level (Boggiani, 1998; Gaucher et al., 2003; Oliveira, 2010) and marking the maximum flooding of the basin. Samples with ichnofossils interpreted as meiofaunal bilaterian burrows were recovered ca. 7 m above the base of the Guaicurus Formation in the Laginha quarry, and elsewhere at the top of the Tamengo Formation (Parry et al., 2017). Synsedimentary structures such as slumps and load structures are interpreted in local places (Fazio et al., 2019), but these have not been related to a possible sedimentary setting such as a slope.

X-ray diffraction analysis (Fazio et al., 2019) of the laminated mudrocks of the Tamengo Formation revealed quartz, smectite, chlorite and illite as major components; the latter three dominate
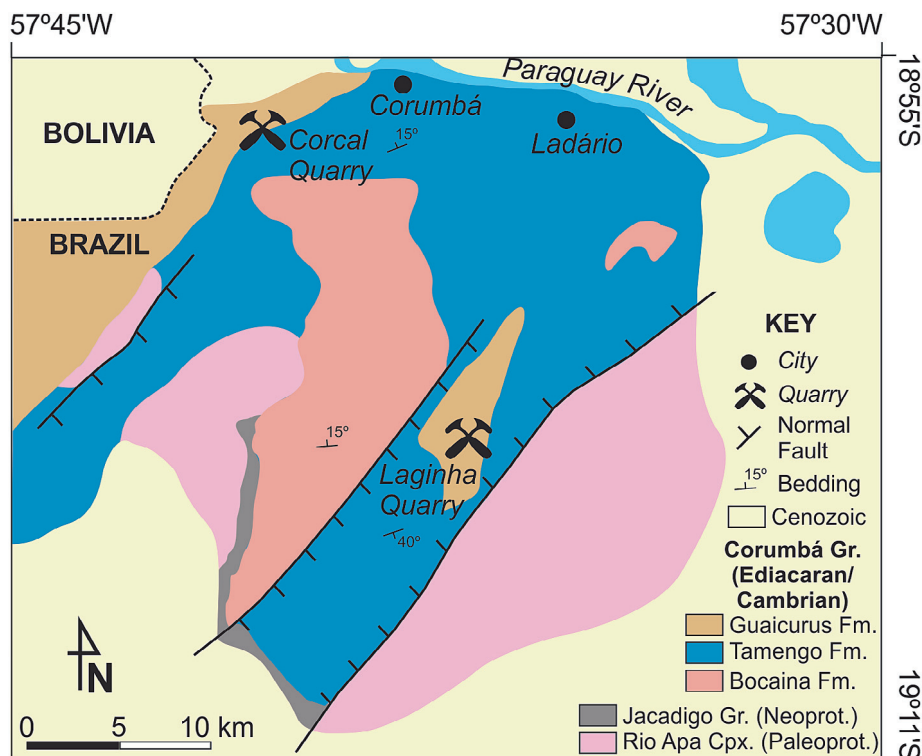
Fig. 2. Simplified geological map of the Corumbá region showing the location of the studied Laginha quarry. For location of the map see Fig. 1. Compiled and modified after Amorim et al. (2020) and Diniz et al. (2021).

the clay fraction. Calcite and dolomite occur in the marl/limestone end-members, and goethite, albite, pyrite and gypsum were detected as minor components. The Guaicurus Formation siliciclastics, on the other hand, broadly lack smectite, with quartz, illite and chlorite along with albite as major to minor components. Additionally, at the boundary between the two units, kaolinite was also detected as a major component in siliciclastic rocks, and 10 m above the contact, gypsum is a major component along with quartz, illite and kaolinite, with vermiculite and calcite as minor components. X-ray fluorescence analysis revealed broadly similar major oxide composition of siliciclastics from both the Tamengo and Guaicurus formations, with SiO_2 and Al_2O_3 varying, respectively, from 47.3 to 65.07 wt.% and from 14.06 to 17.94 wt.%, Fe_2O_3 of 5.14–7.97 wt.%, MgO of 1.71–5.79 wt.% and K_2O of 3.01–5.74 wt.%. The main difference between the two units is the Na_2O contents, less than 0.1 wt.% in the Tamengo and greater than 1.0 wt.% in the Guaicurus siliclastics. CaO contents are normally below 1 wt.% but can reach ca. 5 wt.% in isolated samples of the Guaicurus Formation, while it can reach up to 15 wt.% in samples interleaved in otherwise predominantly siliciclastic intervals of the Tamengo Formation.

The presence of index fossils such as *Cloudina lucianoi* and *Cloudina carinata* (Cortijo et al., 2010) and chemostratigraphic correlations of the C and Sr isotope curves ($^{87}Sr/^{86}Sr$ ratios around 0.7084) assign a terminal Ediacaran age for the Tamengo Formation (Gaucher et al., 2003; Boggiani et al., 2010; Adôrno et al., 2019b). Meiofaunal bilaterian burrows were found in the Guaicurus Formation and in the topmost mudstones interleaved with carbonates of the Tamengo Formation (Parry et al., 2017), indicating that the transition between the two units might span the Ediacaran/Cambrian boundary. This is also supported by organic-walled microfossils (Adôrno et al., 2019a). Furthermore, U-Pb dating of igneous zircons extracted from volcanic ash layers

corroborate this interpretation, with ages of 541.85 ± 0.75 Ma and 542.37 ± 0.28 Ma for the topmost Tamengo Formation and of 555.18 ± 0.3 Ma for the top of the underlying Bocaina Formation (Parry et al., 2017). Thus, deposition of the Tamengo Formation is bracketed between 555 and 542 Ma, whereas the Guaicurus Formation was probably deposited during the early Cambrian.

Inversion of the Corumbá graben system and deformation of the Corumbá Group initiated at around 540–520 Ma, following the last compressional events of the Brasiliano Orogeny due to collision of the Amazon, Rio Apa, and Pampia paleocontinents with the core of western Gondwana (Tohver et al., 2010; McGee et al., 2012).

3. Materials and methods

Samples studied in this work were previously collected and analyzed by Fazio et al. (2019) for petrography, X-ray diffraction and X-ray fluorescence. They correspond to the Laginha quarry section of the previously cited work, including siliciclastic, carbonate and mixed (marl) facies of the Tamengo Formation, and siliciclastic mud/siltstones of the Guaicurus Formation. The data acquired by Fazio et al. (2019) confirm that the samples are within anchizone facies, with clay mineral paragenesis composed of illite + chlorite + quartz in the Guaicurus Fm. and additional smectite in the Tamengo Formation, which are indicative of diagenetic but not of hydrothermal processes. Homogeneous samples, free of visible weathering, veining and other post-depositional alteration features, were crushed to a fine powder in a tungsten carbide shatterbox in preparation for the trace element, total organic carbon, and iron speciation analysis.

Major and trace element analysis was performed by SGS Minerals in Vancouver, Canada following standard 4-acid digestion (HCl/$HClO_4$/HF/HNO_3). Major elements were measured by ICP-OES on a

Perkin Elmer Optima 53000DV or 8300DV, and trace elements were measured by ICP-MS on a Perkin Elmer Elan 9000 or Nexion 300D. United States Geological Survey shale standards SBC-1 and SGR-1 were run alongside samples and results showed good agreement with published values (all data in Supplementary Data Table S1).

Sequential iron extraction of the powdered sample aliquots was performed in the Sedimentary Geochemistry Laboratory of the Stanford Doerr School of Sustainability, and followed the procedures of Poulton and Canfield (2005), with determination of three distinct reactive iron pools: Fe_{carb} (iron in carbonates such as siderite and ankerite), extracted using a 48-h sodium acetate reaction at 50 °C, Fe_{ox} (iron in ferric (oxyhydr)oxide minerals such as ferrihydrite, lepidocrocite, goethite, hematite), using a 2-h sodium dithionite reaction, and Fe_{mag} (mixed-valence phases such as magnetite), using a 6-h ammonium oxalate reaction. Although these extractions are designed to target specific minerals, they are recognized to represent operational extractions and are not perfectly selective, especially the oxalate extraction (Poulton and Canfield, 2005; Slotznick et al., 2020). Iron contents in each pool were determined through the ferrozine spectrophotometric method (Stookey, 1970). The last reactive iron pool, Fe_{py} (iron in pyrite) was determined through the chromium reduction of sulfur (CRS) method (Canfield et al., 1986). Approximately 0.1–0.2 g of powdered sample was added to a reaction vessel, acidified using 20 mL of 6 N HCl, and reacted with 20 mL of 1 M chromous chloride acidified to 0.5 N HCl, heated to near-boiling for 2 h and purged of air using nitrogen gas. The resulting sulfide gas was trapped in a zinc acetate solution and, after filtration, pyrite contents and iron in pyrite were calculated following gravimetric measurement. Samples were run alongside the same set of internal lab standards with consistent results. Detailed methods and estimates of precision can be found in the Supplementary Material of Sperling et al. (2021). Total Fe contents used in the calculation of Fe_{HR}/Fe_T are the ones obtained from SGS Minerals as described above.

An aliquot of the samples was leached in 3 N HCl for 24 h and then sequentially rinsed three times with de-ionized water to remove carbonates. The leached residue was analyzed for Total Organic Carbon on an ECS-8020 elemental analyzer from NC Technologies at the Environmental Measurements Facility, Stanford Doerr School of Sustainability, along with in-house standards for calibration. The organic carbon isotope analysis was carried out at the Stable Isotope Biogeochemistry Laboratory, Stanford University, using a ThermoFisher Scientific EA IsoLink IRMS Elemental Analyzer for CN, interfaced with a ThermoFisher Scientific Delta Q mass spectrometer via a ConFlo IV unit. External precision (1σ) of both carbon and nitrogen isotope data is < 0.1‰, based upon repeated measurements of USGS 40. The $\delta^{13}C_{org}$ values are reported relative to VPDB.

Carbonate carbon and oxygen isotopes for some of the studied samples were formerly presented by Ramos et al. (2022). To this dataset, we add eight new data points from both limestone and marl samples. Inorganic carbon and oxygen isotope analysis were conducted at the Stable Isotope Laboratory (LABISE) of the Department of Geology, Universidade Federal de Pernambuco. Carbonate samples had their CO_2 extracted on a high vacuum line after reaction with phosphoric acid at 25 °C, and cryogenically cleaned. Released CO_2 gas was analyzed for O and C isotopes in a double inlet, triple collector mass spectrometer (VG-Isotech SIRA II), using the BSC reference (Borborema Skarn Calcite) that was calibrated against NBS-20. The external precision, based on multiple standard measurements of NBS-19, was better than 0.1‰ for carbon and oxygen.

Iron speciation, carbonate content, TOC and carbon isotope results are presented in the Supplementary Data Table S2.

4. Results and interpretation

4.1. Interpretation of the iron speciation, trace element and carbon data

Calibration of the iron speciation proxy in modern and Phanerozoic marine sediments has demonstrated that Fe_{HR}/Fe_T (the ratio of highly reactive versus total iron in a given sample) ratios are generally below 0.38 for samples deposited under oxic water column conditions, with an average of 0.14 ± 0.08 for ancient oxic samples (Poulton and Canfield, 2005; Raiswell et al., 2018). Samples that were rapidly deposited may not have had time to gain the authigenic enrichments that the iron speciation proxy attempts to fingerprint, and modern anoxic turbiditic samples have a $Fe_{HR}/Fe_T > 0.2$. Thus, a conservative approach considers samples with $Fe_{HR}/Fe_T \leq 0.22$ as probably deposited under oxic water column conditions and those with $Fe_{HR}/Fe_T \geq 0.38$ under anoxic conditions, with those plotting in between interpreted as ambiguous (Poulton and Canfield, 2011). The ratio of iron in pyrite to the sum of highly reactive iron pools (Fe_{py}/Fe_{HR}) further allows to discrimination of anoxic samples probably deposited under ferruginous (non-sulfidic) or euxinic (anoxic with free sulfide) conditions, with a threshold at about 0.7 based on studies on Phanerozoic sedimentary rocks (März et al., 2008). Recently, these iron speciation thresholds were challenged by Pasquier et al. (2022), who suggested they held little predictive information. However, the compilation used by the authors included a number of samples that would be deemed inappropriate for iron speciation according to Raiswell et al. (2018). Consequently, while it is clear that these thresholds should be revisited, we use the established thresholds from Raiswell et al. (2018). In iron speciation analysis, changes in total iron contents are not as important as the ratios of highly reactive iron to total iron (Fe_{HR}/Fe_T). Thus, although there are lithological controls on some element concentrations, such as an increase in Fe and Al upsection (Supplementary Data Table S2), which is clearly controlled by a lithological change from carbonate-rich facies of the Tamengo Formation to siliciclastics of the Guaicurus Formation, the overall iron speciation trends should not be affected unless there are dramatic changes in detrital Fe_{HR}/Fe_T ratios (discussed further below).

The most prominent feature of the acquired dataset is the sharp decrease, in the Tamengo/Guaicurus transition, of Fe_{HR}/Fe_T values, from ca. 0.7–0.8 throughout the Tamengo Formation to below 0.2 in the Guaicurus Formation, with some intermediate values at around 60 m in stratigraphic height (Fig. 3). This indicates likely anoxic conditions for bottom waters during deposition of the Tamengo Formation, with Fe_{py}/Fe_{HR} around 0.2–0.6 further indicating predominantly ferruginous conditions. Allochtonous *Cloudina* and *Corumbella* fragments found in specific levels within the Tamengo Formation indicates, however, that at least a shallow oxic layer must have existed for these organisms to survive in the platformal setting, before being washed out and transported along with carbonate debris towards the deeper, ferruginous basin. It is important to note that the ferruginous nature of the Tamengo Formation is observed in both carbonate, marl and mudstone samples of this unit, indicating a consistent trend for deposition under anoxic bottom water conditions independent of the lithotypes or total iron contents.

Upon drowning of the basin and deposition of the Guaicurus Formation, however, the redoxcline quickly deepens, eventually reaching the sediment/water interface. While this dramatic change in Fe_{HR}/Fe_T values does occur near a prominent lithological transition, this in itself is unlikely to explain the observed geochemical trend. Iron speciation is based on identifying authigenic enrichments in Fe_{HR} above the normal detrital background input. Thus,
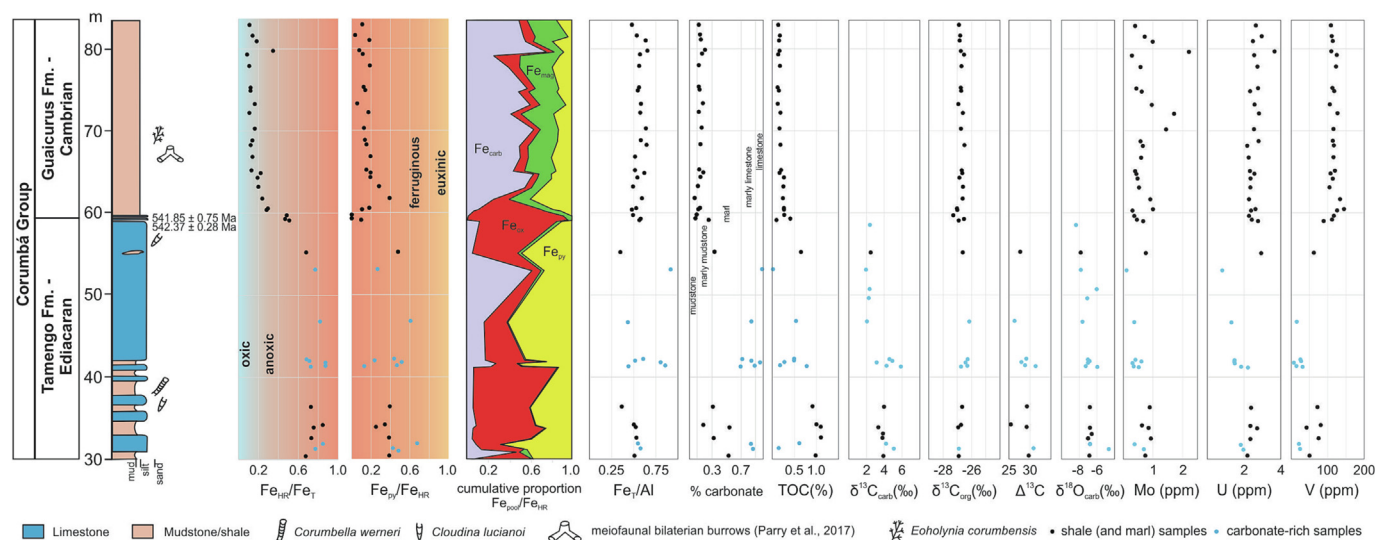
Fig. 3. Chemostratigraphic trends of the Corumbá Group at the Laginha Quarry. Age constraints after Parry et al. (2017). From left to right, geochemical plots represent iron speciation Fe_{HR}/Fe_T and Fe_{py}/Fe_{HR} ratios (with interpretive thresholds derived from Raiswell et al., 2018), the cumulative proportion of different highly reactive iron pools, $Fe_T/$Al ratios, the percentage carbonate as determined gravimetrically from acidification, total organic carbon (TOC) weight percent, inorganic and organic carbon isotope ratios as represented by $\delta^{13}C_{carb}$ (‰) and $\delta^{13}C_{org}$ (‰), respectively, the difference between the inorganic and organic carbon isotope ratios represented by $\Delta^{13}C$, oxygen isotope ratios in the carbonate fraction represented by $\delta^{18}O_{carb}$ (‰) and the relative abundances of redox-sensitive elements molybdenum (Mo), uranium (U) and vanadium (V) in ppm. Enrichment factors and normalizations to TOC or other variables are not presented as most of the concentrations are below or close to typical crustal values, indicating detrital rather than authigenic abundances. Although Parry et al. (2017) described trace fossils at the top of the Tamengo Formation elsewhere, in the Laginha Quarry they only occur at the Guaicurus Formation. Some of the inorganic carbon and oxygen isotope data are compiled from Ramos et al. (2022), with addition of eight new data points as reported in the Supplementary Data Table S2.

it is a 'one-sided test,' with enrichments signifying anoxic conditions but a lack of enrichment being less clear (although most generally this represents a solely detrital iron input under oxic conditions). But, there are conditions in which large enrichments do not develop (reviewed by Chen et al., 2020). If the lithological change was associated with the development of rapid sedimentation, such as in turbiditic systems, there may not be time for authigenic enrichments to develop. Alternatively, if there were essentially zero detrital highly reactive iron delivered to the basin, then a Fe_{HR}/Fe_T of ∼0.15 would represent an authigenic enrichment. Such a situation is extremely rare, though, and does not match the tectonic setting and source areas for the Guaicurus Formation (Boggiani et al., 2010; Fazio et al., 2019). Thus, and as expanded upon in the discussion, it is most likely that the lithological change represents the expression of a common tectonic or paleoceanographic driver that resulted in both lithological change and oxygenation, as opposed to a feature that artifactually resulted in geochemical signals. Although we attempt to keep geochemical and paleontological signals independent in our paleoenvironmental analysis, the presence of the trace fossils does further confirm the geochemical inference of oxygenated bottom waters.

The Fe_T/Al proxy has been used in iron-based redox proxy studies based on the rationale that the enrichment in highly reactive iron observed in anoxic settings should produce a measurable increase in this ratio compared to oxic settings (Lyons and Severmann, 2006). In practice, detecting these enrichments depend on the determination of the detrital baseline Fe_T/Al ratios, which can widely vary throughout the evolution of a sedimentary basin. Suggested typical baselines for oxic conditions vary as widely as ca. 0.47 ± 30, with thresholds for interpreting anoxic conditions above 0.66 or 0.77 (Raiswell et al., 2018). The best approach is to have a clearly defined idea of the local baseline, which is not possible in the single section studied here. In any case, Fe_T/Al in the Laginha Quarry is quite consistent throughout the analyzed section, around 0.5–0.6, although some of the carbonate-rich samples of the Tamengo Formation show some enrichments of 0.8–0.9, consistent with anoxia.

TOC (Total Organic Carbon) contents follow the iron speciation trend, with higher values around 1% in the mudstones of the Tamengo Formation superseded by homogeneously muted low TOC < 0.2% in the Guaicurus Formation. Organic matter was probably highly oxidized before reaching the sediment/water interface during deposition of the latter. Also, bioturbation may have caused bioirrigation, mixing the overlying water and porewater, thus increasing oxygen concentration in sediments and organic matter remineralization. Organic carbon isotope ratios are very consistent with $\delta^{13}C_{org}$ around −27‰ throughout the section. Previous inorganic carbon isotope analysis of the carbonate-rich samples of the Tamengo Formation in the Laginha quarry (Ramos et al., 2022), along with eight new datapoints added to this dataset (Fig. 3), however, indicates a sharp shift with values consistently around +4‰ in the 30–45 m section and +2‰ above that in the Tamengo Formation, with associated $\delta^{18}O$ mostly around −7‰. The combined isotopic data indicate relatively lower $\Delta^{13}C$ (the difference between inorganic and organic $\delta^{13}C$) of ca. 30‰ below and 27‰ above the ca. 45 m mark. In a study using different samples from the Corumbá Group, including different samples from the Laginha Quarry, Spangenberg et al. (2014) also detected this variation on $\Delta^{13}C$ from the middle to the upper portion of the Tamengo Formation. The relatively higher $\Delta^{13}C$ below the 45-m mark is interpreted as part of a major positive carbon isotope excursion (EP2), which the authors interpret as generated by enhanced primary productivity related to increased $p(CO_2)$, nutrient supply and possible changes of the primary producer communities. The drop on $\delta^{13}C_{carb}$ values at the top of the Tamengo Formation would, in this scenario, represent a low productivity period. Other possibilities include one or both records (inorganic and organic $\delta^{13}C$) being affected by diagenesis or not recording open-ocean dissolved inorganic carbon (Ahm and Husson, 2022), changes in O_2-dependent carbon isotope fractionation by phytoplankton (Saltzman et al., 2015; although note the change indicated by the carbon isotopes would be opposite the local redox change we observe), or the influence of detrital organic carbon (Johnston et al., 2012; this may especially explain some of the invariance of

the values in the stratigraphically higher Guaicurus Formation). We also note that this inorganic carbon isotope shift is only constrained by a few data points and a more detailed record from directly paired samples would be informative. This possible change in $\Delta^{13}C$ represents a prospect for future study in the Corumbá Group and other late Ediacaran basins worldwide.

RSE (Redox-Sensitive Element) concentrations are generally muted throughout the section. There is a difference in V contents, which are above 100 ppm in the Guaicurus Formation and below that in the Tamengo Formation. However, Al and Zr versus V concentrations give a well-defined correlation for the Guaicurus shales ($R^2 = 0.6$; not shown), thus suggesting a detrital rather than authigenic origin for V enrichment. U is homogeneous throughout, with values between 2 and 3 ppm for both units. Mo concentrations are muted in both units, with only slightly higher concentrations in the Guaicurus Formation, but mainly below the upper crustal average of 1.1 ppm (Rudnick and Gao, 2003); thus, commonly used calculations to determine the authigenic fractions of Mo and U using crustal values and estimates for detrital inputs return negative values and are not presented here. Metal/aluminum input to the basin was probably lower than average (although not unexpectedly so given observed regional variation in modern basins; Cole et al., 2020), and the abundances in the sediments observed are primarily detrital and not authigenic (note that minor authigenic enrichment may be present in the Tamengo Formation, but the overall signal is dominantly detrital). For this reason, we do not present metal/TOC or other similar plots, as they would track the plot of a biogeochemically conservative element (e.g. Al/TOC) because there is no authigenic enrichment, only detrital input. These muted trace metal concentrations support deposition under non-sulfidic bottom water conditions. The low Fe_{py}/Fe_{HR} values corroborate this interpretation, indicating the lack of free sulfide in the water column when bottom waters were anoxic.

A more nuanced interpretation of the changes in bottom water redox conditions can be obtained by analyzing the stratigraphic distribution of the individual reactive iron pools (Fig. 3). In this distribution, it is clear that Fe_{Ox} dominates the highly reactive iron pool during deposition of the Tamengo Formation, followed by Fe_{Py}, while Fe_{carb} is the main reactive phase during deposition of the Guaicurus Formation, followed by Fe_{mag}. These trends can be explained by a model (Fig. 4) that starts with a stratified basin with an oxic shallow carbonate platform adjacent to anoxic ferruginous deeper waters, with occasional input of relatively siliciclastic sediment during deposition of the Tamengo Formation. Under these conditions, iron sourced from the continent was intensely cycled through the water column due to its abundant availability to react. During deposition of the Tamengo Formation, the anoxic but non-sulfidic deeper waters would allow upwelling of Fe and precipitation of Fe_{HR} (specifically iron oxides) in the oxic shallow waters, elevating Fe_{HR}/Fe_T and generating high Fe_{ox}/Fe_{HR}, with no accompanying trace metal enrichment. Then, quick drowning of the platform along with deepening of the redoxcline led to deposition under oxic bottom waters observed in the Guaicurus Formation, with bioturbation and bioirrigation. Since the sediment–water interface was oxygenated, Fe_{carb} increase was probably caused by iron carbonate precipitation through organic matter remineralization via Fe(III) and iron reduction during early diagenesis. Thus, reducing porewaters led to transfer of Fe oxides to reduced Fe phases. Slotznick et al. (2020) have recently demonstrated that high Fe_{mag} may actually represent the formation (and subsequent extraction) of clays such as berthierine and chamosite that form in iron-rich pore waters. Thus, we interpret the Guaicurus Formation to have been deposited under oxic conditions (such that authigenic enrichments in Fe_{HR} relative to Fe_T did not develop), but with early diagenesis dominated by iron reduction and little sulfate reduction, such that released Fe^{2+} formed early diagenetic carbon-

ates and clays rather than pyrite. The studied samples in fact are shales with ca. 10%–15% carbonate content, which likely represent carbonate cements formed during early diagenesis.

### 4.2. Redox trends across the Ediacaran/Cambrian transition in the Corumbá basin

The new data presented here, in conjuction with paleontological data, indicates deposition of the Tamengo Formation occurred under a stratified water column with a shallow oxic layer capping a deep ferruginous basin over a diffuse redoxcline. This seems to be a rather common situation for late Ediacaran basins throughout the world, and pioneer biomineralizing organisms such as *Cloudina* and *Corumbella* seemed to have thrived under fluctuating redox conditions that would allow fleeting colonization of shallow water platforms (Wood et al., 2015; Tostevin et al., 2016; Bowyer et al., 2017; Jin et al., 2018; Caxito et al., 2021). Then, an important change in redox conditions accompanied a major paleoenvironmental change, with flooding of the basin and transgression of deep-water sediments over the shallow platform coinciding with deepening of the redoxcline and oxic bottom water conditions during deposition of the Guaicurus Formation. Our model for redox structure of the Corumbá basin, based mainly on iron speciation data, is consistent with previous suggestions based on nitrogen isotopes in the Tamengo Formation with $\delta^{15}N_{kerogen}$ between $-3.3‰$ and $+3.1‰$, recording the regional signal of N_2-fixation and/or ammonium assimilation expected for redox-stratified basins (Ader et al., 2014; Spangenberg et al., 2014), and of deposition of the Guaicurus Formation under oxic conditions with eukaryotic algae as the main primary producers based on trace elements and biomarker data, respectively (Spangenberg et al., 2014).

Notably, this redox change occurs at the level where small but complex meiofaunal animal burrows, attributed to a nematoid-like organism, occur in the stratigraphic record of the Corumbá Group (Parry et al., 2017). Meiofaunal bioturbation is also recognized at multiple localities in the coeval Nama Group of Namibia (Darroch et al., 2021) and may have become widespread at this time (although it is noted that many of these 'meiofaunal' trace fossils were likely made by organisms slightly larger than the standard biological definition of passing through a 500 µm sieve).

Oxygenated bottom waters were a necessary (if not necessarily sufficient, with other possible factors such as nutrient availability, pH, salinity and temperature controlling biodiversity in distinct Ediacaran–Cambrian basins) constraint on the development of complex ecosystems on the deep seafloor, which lead to a substrate or "agronomical" evolution characterized by the increase of vertically-oriented burrows in early Cambrian trace fossils (Seilacher and Pflüger, 1994), such as those observed in the Corumbá Group (Parry et al., 2017). The increase in vertical bioturbation, either for feeding or protection against predation, would have allowed mixing of oxygen and water to deeper levels within the seafloor sediments, restricting sulfate-reducing bacteria and their toxic sulfide emissions to progressively deeper layers and re-oxidizing buried sulfide phases. This is hypothesized by Canfield and Farquhar (2009) to have resulted in rising seawater sulfate levels, which in turn might have facilitated internal marine recycling of key nutrients such as phosphorus (Laakso et al., 2020).

Relating such global biogeochemical changes to the advent of bioturbation (and especially to the effects of meiofaunal organisms), while intriguing, remains complicated. First, the activities of bioturbators often have complex effects on geochemical cycles, and it is clear that not all bioturbation is equal (see for instance Tarhan et al., 2021; Cribb et al., 2023). Second, although meiofauna are certainly involved in many benthic processes (Schratzberger and Ingels, 2018), their biogeochemical effect compared to macrofaunal bioturbation are both different in terms of decomposition
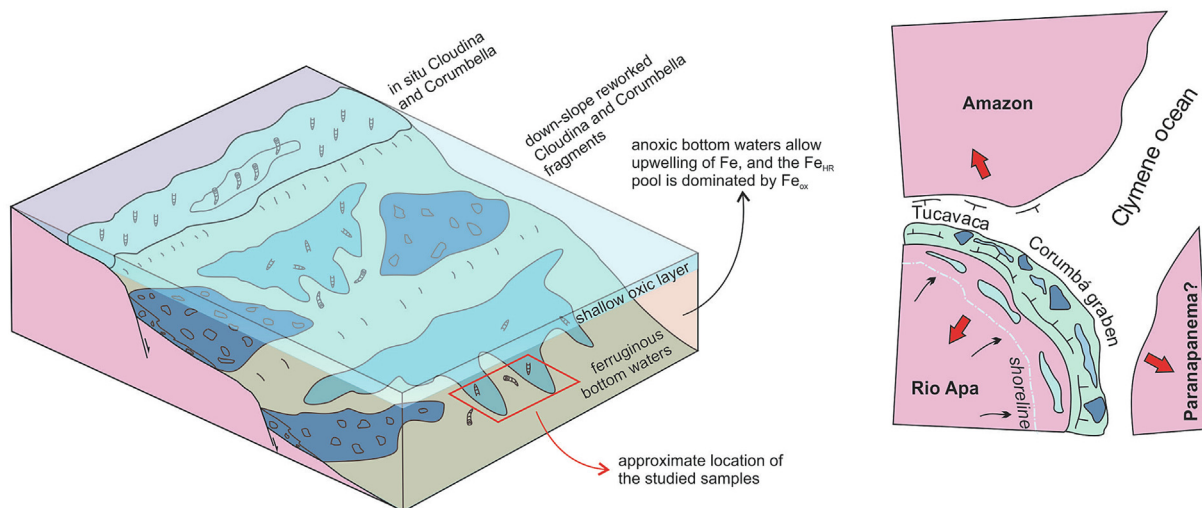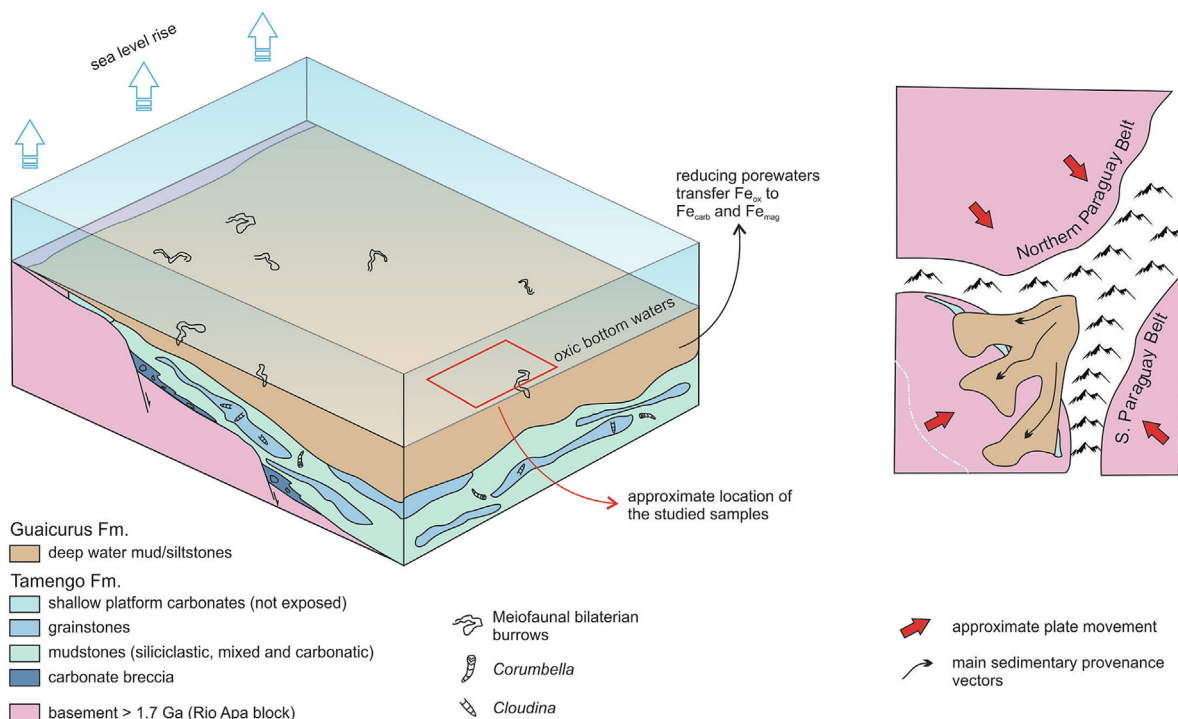
Fig. 4. Models for the deposition of the Tamengo and Guaicurus formations at the Ediacaran–Cambrian transition (left) and tectonic configuration of the basin and adjacent continental blocks (right), with red arrows indicating general movement of the involved paleocontinental blocks and black arrows indicating main sedimentary provenance vectors. The approximate location of the studied samples is indicated by the red rectangles. (A) Deposition of the Tamengo Formation in the late Ediacaran (ca. 550–540 Ma) occurred in a stratified basin with a shallow oxic layer where biomineralizing organisms such as *Cloudina* and *Corumbella* thrived. Shell fragments of these were transported down-slope and deposited under ferruginous bottom water conditions. During this time frame, the Amazon, Rio Apa and Paranapanema paleocontinents were rifted apart, and the basin mainly sourced the adjacent Rio Apa block. (B) Deposition of the Guaicurus Formation in the early Cambrian occurred during a major transgression, flooding the basin while the redoxcline was drastically deepened, generating oxic bottom water conditions where bioturbating organisms thrived. Detrital zircon U-Pb age spectra indicates that during this time frame, the basin sourced the mountainous areas related to the Brasiliano Orogen to the west, due to collision of the Amazon, Rio Apa and Paranapanema paleocontinents. (For interpretation of the references to colour in this figure legend, the reader is referred to the web version of this article.)

process and far less pronounced (Aller and Aller, 1992). Thus, much remains to be learned regarding the effect of early bioturbators on biogeochemical cycles. Nonetheless, the results here clearly demonstrate a temporal relationship between the appearance of oxygenated bottom waters in the Corumbá basin and the spread of meiofaunal trace fossils.

The next important question to be asked is why bottom waters became fully oxygenated coeval with sea level rise and deposition of the Guaicurus Formation, stabilizing deeper water communities of complex organisms especially in this time frame. Available detrital zircon U-Pb data indicates that provenance of the Tamengo Formation is dominated by 900 to 1900 Ma sources, which can all

be found within the Rio Apa block (Babinski et al., 2008), which is the immediate basement of the Corumbá basin. Samples from the Guaicurus Formation, on the other hand, are dominated by late Neoproterozoic detrital zircons, peaking at ca. 620–650 Ma and with a maximum depositional age at 543 ± 11 Ma (McGee et al., 2018). This indicates a very important provenance shift between the two units (Fig. 4). While the Tamengo Formation was deposited in a rift setting and sourced only cratonic basement, the Guaicurus Formation shows a strong influence of the sources located in the then recently uplifted Brasiliano mountains to the east. This mountain range resulted from the collision of the Amazon/Rio Apa paleocontinents with the amalgamated remainder of western Gondwana as the final orogenesis that consolidated this paleocontinent in the early Cambrian (Tohver et al., 2010; McGee et al., 2012; Caxito et al., 2021). A similar interpretation of deposition of the upper Corumbá Group in a foreland basin setting was put forward by Campanha et al. (2011), with a difference that these authors interpreted the Tamengo Formation as also deposited in a foreland setting.

One possibility is that erosion of the recently uplifted mountainous regions of the Brasiliano/PanAfrican orogeny would have led to a higher sedimentation rate and enhanced organic carbon burial in the adjacent foreland basins, leading to a global surplus in oxygen that could not back-react to form CO_2 (Squire et al., 2006; Campbell and Squire, 2010). Another possible explanation is that a formerly relatively isolated graben basin with a stratified redox framework, where the Tamengo Formation was deposited, became oceanographically connected to the open ocean, upon transgression and deposition of the Guaicurus Formation. Note that the proxies used here are better at determining 'oxic' versus 'anoxic' conditions rather than the degree of oxygenation of seawater (see discussion in Haxen et al., 2023), and a greater connection to the open ocean may have allowed for the transit of increasingly oxygenated seawater even if modern-style oxygenation of deeper waters was a later Paleozoic phenomenon (Sperling et al., 2015). Put differently, while this study provides new key data points regarding oxygen and early animal evolution in the Corumbá basin—specifically the temporal correlation of oxygenation and trace fossil appearances—further study is required to determine if the cause of oxygenation is global (i.e., a planetary-scale rise of atmospheric oxygen) or regional (i.e., controlled by tectonic and/or paleoceanographic factors).

5. Conclusions

The new data presented here adds to a growing dataset indicating that oceanic redox conditions were highly heterogeneous in the key biological interval of the Ediacaran/Cambrian transition. In the Corumbá basin of western Brazil, as in similar basins throughout the world, early biomineralizing late Ediacaran organisms such as *Cloudina* and *Corumbella* seem to have thrived under a shallow surficial oxic layer, while deeper oceanic realms were broadly ferruginous and hampered colonization of bottom dwellers. Fragments of these organisms are preserved in the reworked mixed carbonate-siliciclastic deposits of the Tamengo Formation (555–541 Ma), developed in a rift basin that sourced the local Rio Apa block Archean to Proterozoic igneous and metamorphic basement rocks. In contrast, the overlying siliciclastics of the Guaicurus Formation (<541 Ma) were deposited under a completely oxic water column in a foreland basin setting that sourced the recently uplift Ediacaran/Cambrian Brasiliano mountains to the east, which facilitated the proliferation of bioturbating animals, including

bilaterian burrowers that promoted vertical mixing of the underlying sedimentary beds. The cause for this abrupt redox shift between the two units and straddling approximately the Proterozoic/Phanerozoic transition is unknown and might have been influenced by tectonic and/or paleogeographic factors, but the relationship between local oxygenation and trace fossil appearance is clear.

CRediT authorship contribution statement

Fabricio A. Caxito: Conceptualization, Methodology, Investigation, Data curation, Writing – original draft, Visualization, Project administration, Funding acquisition. **Erik Sperling:** Conceptualization, Methodology, Validation, Writing – review & editing, Resources, Funding acquisition. **Gabriella Fazio:** Resources, Writing – review & editing, Visualization. **Rodrigo Rodrigues Adorno:** Resources, Writing – review & editing, Visualization. **Matheus Denezine:** Resources, Writing – review & editing, Visualization. **Dermeval Aparecido Do Carmo:** Resources, Writing – review & editing, Visualization. **Martino Giorgioni:** Resources, Writing – review & editing, Visualization. **Gabriel J. Uhlein:** Resources, Writing – review & editing, Validation, Data curation. **Alcides N. Sial:** Resources, Methodology, Writing – review & editing, Validation, Data curation.

Declaration of Competing Interest

The authors declare that they have no known competing financial interests or personal relationships that could have appeared to influence the work reported in this paper.

Acknowledgments

Appendix A. Supplementary data

Supplementary data to this article can be found online at https://doi.org/10.1016/j.gsf.2024.101810.

References

Ader, M., Sansjofre, P., Halverson, G.P., Busigny, V., Trindade, R.I., Kunzmann, M., Nogueira, A.C., 2014. Ocean redox structure across the late neoproterozoic oxygenation event: a nitrogen isotope perspective. Earth Planet. Sci. Lett. 396, 1–13.

Adorno, R.R., Carmo, D.A.d., Germs, G., Walde, D.H.G., Denezine, M., Boggiani, P.C., Sousa e Silva, S.C., Vasconcelos, J.R., Tobias, T.C., Guimarães, E.M., Vieira, L.C., Figueiredo, M.F., Moraes, R., Caminha, S.A., Suarez, P.A.Z., Rodrigues, C.V., Caixeta, G.M., Pinho, D., Schneider, G., Muyamba, R., 2017. Cloudina lucianoi (Beurlen & Sommer, 1957), Tamengo Formation, Ediacaran, Brazil: Taxonomy, analysis of stratigraphic distribution and biostratigraphy. Precambrian Res. 301, 19–35. https://doi.org/10.1016/j.precamres.2017.08.023.

Adôrno, R.R., Walde, D.H.G., Do Carmo, D.A., Denezine, M., Cortijo, I., Sanchez, E.A. M., Tobias, T.C., Fazio, G., Warren, L.V., Erdtmann, B.D., Cai, Y., Giorgioni, M., Ramos, M.E.A.F., Baptista, M.C., Guimarães, E.M., Figueiredo, M.F., Germs, G.J., 2019a. Palaeontological analyses across the Ediacaran-Cambrian boundary, Upper Corumbá Group, Brazil. Estud. Geol. 75. https://doi.org/10.3989/EGEOL.43586.549.

Adôrno, R.R., Walde, D.H.G., Erdtmann, B.D., Denezine, M., Cortijo, I., Do Carmo, D.A., Giorgioni, M., Ramos, M.E.A.F., Fazio, G., 2019b. First occurrence of Cloudina carinata Cortijo et al., 2010 in South America, Tamengo Formation, Corumbá Group, upper Ediacaran of Midwestern. Estud. Geol. 75, 10–13. https://doi.org/10.3989/EGEOL.43587.550.

Ahm, A.S., Husson, J., 2022. Local and Global Controls on Carbon Isotope Chemostratigraphy. Cambridge University Press.

Aller, R.C., Aller, J.Y., 1992. Meiofauna and solute transport in marine muds. Limnol. Oceanogr. 37, 1018–1033. https://doi.org/10.4319/LO.1992.37.5.1018.

Almeida, F.F.M., 1965. Geologia da Serra da Bodoquena (Mato Grosso), Brasil. Boletim da Divisão de Geologia e Mineralogia, vol. 219. Departamento Nacional de Produção Mineral – DNPM (in Spanish).

Amorim, K.B., Afonso, J.W.L., Leme, J.d.M., Diniz, C.Q.C., Rivera, L.C.M., Gómez-Gutiérrez, J.C., Boggiani, P.C., Trindade, R.I.F., 2020. Sedimentary facies, fossil distribution and depositional setting of the late Ediacaran Tamengo Formation (Brazil). Sedimentology 67, 3422–3450. https://doi.org/10.1111/sed.12749.

Babinski, M., Boggiani, P.C., Fanning, C.M., Fairchild, T.R., Simon, C.M., Sial, A.N., 2008. U-Pb SHRIMP geochronology and isotope chemostratigraphy (C, O, Sr) of the Tamengo Formation, southern Paraguay belt, Brazil, in: South American Symposium on Isotope Geology. Buenos Aires.

Beurlen, K., Sommer, F.W., 1957. Observações estratigráficas e paleontológicas sobre o calcário de Corumbá. Bol. Geol. e Mineral. - DNPM 168 (in Spanish).

Boggiani, P.C., 1998. Análise estratigráfica da Bacia Corumbá (Neoproterozóico) - Mato Grosso do Sul. Universidade De São Paulo (in Spanish).

Boggiani, P.C., Gaucher, C., Sial, A.N., Babinski, M., Simon, C.M., Riccomini, C., Ferreira, V.P., Fairchild, T.R., Sial, A.N., Babinski, M., Simon, C.M., Riccomini, C., Ferreira, V.P., Fairchild, T.R., 2010. Chemostratigraphy of the Tamengo Formation (Corumbá Group, Brazil): A contribution to the calibration of the Ediacaran carbon-isotope curve. Precambrian Res. 182, 382–401. https://doi.org/10.1016/j.precamres.2010.06.003.

Bowyer, F.T., Shore, A.J., Wood, R.A., Alcott, L.J., Thomas, A.L., Butler, I.B., Curtis, A., Hainanna, S., Curtis-Walcott, S., Penny, A.M., Poulton, S.W., 2020. Regional nutrient decrease drove redox stabilisation and metazoan diversification in the late Ediacaran Nama Group, Namibia. Sci. Rep. 10, 1–11. https://doi.org/10.1038/s41598-020-59335-2.

Bowyer, F., Wood, R.A., Poulton, S.W., 2017. Controls on the evolution of Ediacaran metazoan ecosystems: A redox perspective. Geobiology 15, 516–551. https://doi.org/10.1111/gbi.12232.

Bowyer, F.T., Zhuravlev, A.Y., Wood, R., Shields, G.A., Zhou, Y., Curtis, A., Poulton, S. W., Condon, D.J., Yang, C., Zhu, M., 2022. Calibrating the temporal and spatial dynamics of the Ediacaran - Cambrian radiation of animals. Earth-Science Rev. 225, 103913. https://doi.org/10.1016/j.earscirev.2021.103913.

Campanha, G.A. da C., Boggiani, P.C., Sallun Filho, W., Sá, F.R. de, Zuquim, M. de P.S., Piacentini, T., 2011. A faixa de dobramento Paraguai na Serra da Bodoquena e depressão do Rio Miranda, Mato Grosso do Sul. Geol. USP. Série Científica 11, 79–96. https://doi.org/10.5327/Z1519-874X2011000300005 (in Spanish).

Campbell, I.H., Squire, R.J., 2010. The mountains that triggered the Late Neoproterozoic increase in oxygen: The Second Great Oxidation Event. Geochim. Cosmochim. Acta 74, 4187–4206. https://doi.org/10.1016/j.gca.2010.04.064.

Canfield, D.E., Farquhar, J., 2009. Animal evolution, bioturbation, and the sulfate concentration of the oceans. Proc. Natl. Acad. Sci. u.s.a. 106, 8123–8127. https://doi.org/10.1073/pnas.0902037106.

Canfield, D.E., Raiswell, R., Westrich, J.T., Reaves, C.M., Berner, R.A., 1986. The use of chromium reduction in the analysis of reduced inorganic sulfur in sediments and shales. Chem. Geol. 54, 149–155. https://doi.org/10.1016/0009-2541(86)90078-1.

Caxito, F.A., Uhlein, G.J., Uhlein, A., Pedrosa-Soares, A.C., Kuchenbecker, M., Reis, H., Sial, A.N., Ferreira, V.P., Alvarenga, C.J.S., Santos, R.V., Vieira, L.C., Dantas, E., Babinski, M., Trindade, R., Boggiani, P.C., Warren, L., Hippertt, J.P., Sotero, M.P., Rodrigues de Paula, J., 2019. Isotope stratigraphy of Precambrian sedimentary rocks from Brazil: Keys to unlock Earth's hydrosphere, biosphere, tectonic, and climate evolution. Stratigraphy & Timescales 4, 73–132. https://doi.org/10.1016/bs.sats.2019.08.002.

Caxito, F.A., Lana, C., Frei, R., Uhlein, G.J., Sial, A.N., Dantas, E.L., Pinto, A.G., Campos, F.C., Galvão, P., Warren, L.V., Okubo, J., Ganade, C.E., 2021. Goldilocks at the dawn of complex life: mountains might have damaged Ediacaran-Cambrian ecosystems and prompted an early Cambrian greenhouse world. Sci. Rep. 11, 1–15. https://doi.org/10.1038/s41598-021-99526-z.

Chen, X., Li, M., Sperling, E.A., Zhang, T., Zong, K., Liu, Y., Shen, Y., 2020. Mesoproterozoic paleo-redox changes during 1500–1400 Ma in the Yanshan Basin, North China. Precambrian Res. 347, 105835. https://doi.org/10.1016/J.PRECAMRES.2020.105835.

Clarkson, M.O., Poulton, S.W., Guilbaud, R., Wood, R.A., 2014. Assessing the utility of Fe/Al and Fe-speciation to record water column redox conditions in carbonate-rich sediments. Chem. Geol. 382, 111–122. https://doi.org/10.1016/j.chemgeo.2014.05.031.

Cole, D.B., Mills, D.B., Erwin, D.H., Sperling, E.A., Porter, S.M., Reinhard, C.T., Planavsky, N.J., 2020. On the co-evolution of surface oxygen levels and animals. Geobiology 18, 260–281. https://doi.org/10.1111/gbi.12382.

Cortijo, I., Martí Mus, M., Jensen, S., Palacios, T., 2010. A new species of Cloudina from the terminal Ediacaran of Spain. Precambrian Res. 176, 1–10. https://doi.org/10.1016/j.precamres.2009.10.010.

Cribb, A.T., van de Velde, S.J., Berelson, W.M., Bottjer, D.J., Corsetti, F.A., 2023. Ediacaran-Cambrian bioturbation did not extensively oxygenate sediments in shallow marine ecosystems. Geobiology 21 (4), 435–453. https://doi.org/10.1111/gbi.12550.

Dahl, T.W., Connelly, J.N., Kouchinsky, A., Gill, B.C., Månsson, S.F., Bizzarro, M., 2017. Reorganisation of earth's biogeochemical cycles briefly oxygenated the oceans 520 myr ago. Geochemical Perspect. Lett. 10, 210–220. https://doi.org/10.7185/GEOCHEMLET.1724.

Darroch, S.A.F., Cribb, A.T., Buatois, L.A., Germs, G.J.B., Kenchington, C.G., Smith, E.F., Mocke, H., O'Neil, G.R., Schiffbauer, J.D., Maloney, K.M., Racicot, R.A., Turk, K.A., Gibson, B.M., Almond, J., Koester, B., Boag, T.H., Tweedt, S.M., Laflamme, M., 2021. The trace fossil record of the Nama Group, Namibia: Exploring the terminal Ediacaran roots of the Cambrian explosion. Earth-Science Rev. 212, 103435. https://doi.org/10.1016/J.EARSCIREV.2020.103435.

Diniz, C.Q.C., de M. Leme, J., Boggiani, P.C., 2021. New Species of Macroalgae from Tamengo Formation, Ediacaran, Brazil. Front. Earth Sci. 9, 1–11. https://doi.org/10.3389/feart.2021.748876.

Erwin, D.H., Laflamme, M., Tweedt, S.M., Sperling, E.A., Pisani, D., Peterson, K.J., 2011. The Cambrian conundrum: Early divergence and later ecological success in the early history of animals. Science 334 (6059), 1091–1097. https://doi.org/10.1126/science.1206375.

Fazio, G., Guimarães, E.M., Walde, D.W.G., Carmo, D.A.d., Adorno, R.R., Vieira, L.C., Denezine, M., da Silva, C.B., de Godoy, H.V., Borges, P.C., Pinho, D., 2019. Mineralogical and chemical composition of Ediacaran-Cambrian pelitic rocks of The Tamengo and Guaicurus formations, (Corumbá Group - MS, Brazil): Stratigraphic positioning and paleoenvironmental interpretations. J. South Am. Earth Sci. 90, 487–503. https://doi.org/10.1016/J.JSAMES.2018.11.025.

Fernandes, H.A., Boggiani, P.C., Afonso, J.W.L., Amorim, K.B., Trindade, R.I.F., 2022. Sedimentary and tectonic breccias at the base of the Ediacaran Tamengo Formation (Corumbá Group): a comparative study. Brazilian Journal of Geology 52, e20210062.

Gaucher, C., Boggiani, P.C., Sprechmann, P., Sial, A.N., Fairchild, T.R., 2003. Integrated correlation of the Vendian to Cambrian Arroyo del Soldado and Corumba groups (Uruguay and Brazil). Precambrian Res. 120, 241–278. https://doi.org/10.1016/s0301-9268(02)00140-7.

Hahn, G., Hahn, R., Leonardos, O.H., Pflug, H.D., Walde, D.H.G., 1982. Körperlich erhaltene Scyphozoen-Reste aus dem Jungpräkambrium Brasiliens. Geol. Palaeontol. 16, 1–18.

Haxen, E.R., Schovsbo, N.H., Nielsen, A.T., Richoz, S., Loydell, D.K., Posth, N.R., Canfield, D., Hammarlund, E.U., 2023. "Hypoxic" Silurian oceans suggest early animals thrived in a low-O_2 world. Earth Planet. Sci. Lett. 622, 118416.

He, T., Zhu, M., Mills, B.J.W., Wynn, P.M., Zhuravlev, A.Y., Tostevin, R., Pogge von Strandmann, P.A.E., Yang, A., Poulton, S.W., Shields, G.A., 2019. Possible links between extreme oxygen perturbations and the Cambrian radiation of animals. Nat. Geosci. 12, 468–474. https://doi.org/10.1038/s41561-019-0357-z.

Hoffman, P.F., Abbot, D.S., Ashkenazy, Y., Benn, D.I., Brocks, J.J., Cohen, P.A., Cox, G. M., Creveling, J.R., Donnadieu, Y., Erwin, D.H., Fairchild, I.J., Ferreira, D., Goodman, J.C., Halverson, G.P., Jansen, M.F., Le Hir, G., Love, G.D., Macdonald, F.A., Maloof, A.C., Partin, C.A., Ramstein, G., Rose, B.E.J.J., Rose, C.V., Sadler, P.M., Tziperman, E., Voigt, A., Warren, S.G., 2017. Snowball Earth climate dynamics and Cryogenian geology-geobiology. Sci. Adv. 3, e1600983. https://doi.org/10.1126/sciadv.1600983.

Jin, C., Li, C., Algeo, T.J., O'Connell, B., Cheng, M., Shi, W., Shen, J., Planavsky, N.J., 2018. Highly heterogeneous "poikiloredox" conditions in the early Ediacaran Yangtze Sea. Precambrian Res. 311, 157–166. https://doi.org/10.1016/j.precamres.2018.04.012.

Johnston, D.T., Macdonald, F.A., Gill, B.C., Hoffman, P.F., Schrag, D.P., 2012. Uncovering the Neoproterozoic carbon cycle. Nature 483 (7389), 320–323.

Jones, J.P., 1985. The southern border of the Guaporé Shield in Wesern Brazil and Bolivia: an interpretation of its geologic evolution. Precambrian Res. 28, 111–135.

Laakso, T.A., Sperling, E.A., Johnston, D.T., Knoll, A.H., 2020. Ediacaran reorganization of the marine phosphorus cycle. Proc. Natl. Acad. Sci. u.s.a. 117, 1–7. https://doi.org/10.1073/pnas.1916738117.

Lyons, T.W., Severmann, S., 2006. A critical look at iron paleoredox proxies: New insights from modern euxinic marine basins. Geochim. Cosmochim. Acta 70, 5698–5722. https://doi.org/10.1016/J.GCA.2006.08.021.

März, C., Poulton, S.W., Beckmann, B., Küster, K., Wagner, T., Kasten, S., 2008. Redox sensitivity of P cycling during marine black shale formation: dynamics of sulfidic and anoxic, non-sulfidic bottom waters. Geochim. Cosmochim. Acta 72 (15), 3703–3717.

McGee, B., Collins, A.S., Trindade, R.I.F., 2012. G'day Gondwana - the final accretion of a supercontinent: U-Pb ages from the post-orogenic São Vicente Granite, northern Paraguay Belt, Brazil. Gondwana Res. 21, 316–322. https://doi.org/10.1016/j.gr.2011.04.011.

McGee, B., Babinski, M., Trindade, R., Collins, A.S., 2018. Tracing final Gondwana assembly: Age and provenance of key stratigraphic units in the southern Paraguay Belt, Brazil. Precambrian Res. 307, 1–33. https://doi.org/10.1016/j.precamres.2017.12.030.

Merdith, A.S., Collins, A.S., Williams, S.E., Pisarevsky, S., Foden, J.D., Archibald, D.B., Blades, M.L., Alessio, B.L., Armistead, S., Plavsa, D., Clark, C., Müller, R.D., 2017. A full-plate global reconstruction of the Neoproterozoic. Gondwana Res. 50, 84–134. https://doi.org/10.1016/j.gr.2017.04.001.

Mills, D.B., Canfield, D.E., 2014. Oxygen and animal evolution: Did a rise of atmospheric oxygen "trigger" the origin of animals? Bioessays 36, 1145–1155. https://doi.org/10.1002/BIES.201400101.

Och, L.M., Shields-Zhou, G.A., 2012. The Neoproterozoic oxygenation event: environmental perturbations and biogeochemical cycling. Earth-Science Rev. 110, 26–57. https://doi.org/10.1016/j.earscirev.2011.09.004.

Oliveira, R.S., 2010. Depósitos de rampa carbonática Ediacarana do Grupo Corumbá, região de Corumbá. Universidade Federal do Pará, Mato Grosso do Sul. (in Spanish).

Pacheco, M.L.F., Galante, D., Rodrigues, F., de M. Leme, J., Bidola, P., Hagadorn, W., Stockmar, M., Herzen, J., Rudnitzki, I.D., Pfeiffer, F., Marques, A.C., 2015. Insights into the skeletonization, lifestyle, and affinity of the unusual Ediacaran fossil Corumbella. PLoS One 10 (3), e0114219.

Parry, L.A., Boggiani, P.C., Condon, D.J., Garwood, R.J., de M. Leme, J., McIlroy, D., Brasier, M.D., Trindade, R., Campanha, G.A.C., Pacheco, M.L.A.F., Diniz, C.Q.C., Liu, A.G., 2017. Ichnological evidence for meiofaunal bilaterians from the terminal Ediacaran and earliest Cambrian of Brazil. Nat. Ecol. Evol. 1, 1455–1464. https://doi.org/10.1038/s41559-017-0301-9.

Pasquier, V., Fike, D.A., Révillon, S., Halevy, I., 2022. A global reassessment of the controls on iron speciation in modern sediments and sedimentary rocks: A dominant role for diagenesis. Geochim. Cosmochim. Acta 335, 211–230. https://doi.org/10.1016/J.GCA.2022.08.037.

Poulton, S.W., Canfield, D.E., 2005. Development of a sequential extraction procedure for iron: implications for iron partitioning in continentally derived particulates. Chem. Geol. 214, 209–221. https://doi.org/10.1016/j.chemgeo.2004.09.003.

Poulton, S.W., Canfield, D.E., 2011. Ferruginous conditions: A dominant feature of the ocean through Earth's history. Elements 7, 107–112. https://doi.org/10.2113/gselements.7.2.107.

Raiswell, R., Hardisty, D.S., Lyons, T.W., Canfield, D.E., Owens, J.D., Planavsky, N.J., Poulton, S.W., Reinhard, C.T., 2018. The iron paleoredox proxies: A guide to the pitfalls, problems and proper practice. Am. J. Sci. 318, 491–526. https://doi.org/10.2475/05.2018.03.

Ramos, M.E.A.F., Giorgioni, M., Walde, D.H.G., Carmo, D.A.d., Fazio, G., Vieira, L.C., Denezine, M., Santos, R.V., Adôrno, R.R., Lage Guida, L., 2022. New Facies Model and Carbon Isotope Stratigraphy for an Ediacaran Carbonate Platform From South America (Tamengo Formation—Corumbá Group, SW Brazil). Front. Earth Sci. 10, 1–24. https://doi.org/10.3389/feart.2022.749066.

Rudnick, R.L., Gao, S., 2003. Composition of the Continental Crust. Treatise on Geochemistry 3–9, 1–64. https://doi.org/10.1016/B0-08-043751-6/03016-4.

Saltzman, M.R., Edwards, C.T., Adrain, J.M., Westrop, S.R., 2015. Persistent oceanic anoxia and elevated extinction rates separate the Cambrian and Ordovician radiations. Geology 43, 807–810. https://doi.org/10.1130/G36814.1.

Schratzberger, M., Ingels, J., 2018. Meiofauna matters: the roles of meiofauna in benthic ecosystems. J. Exp. Mar. Bio. Ecol. 502, 12–25. https://doi.org/10.1016/J.JEMBE.2017.01.007.

Seilacher, A., Pflüger, F., 1994. From biomats to benthic agriculture: A biohistoric revolution. In: Krumbein, W.E., Peterson, D.M., Stal, L.J. (Eds.), Biostabilization of Sediments. Bibliotheks und Informationssystem der Carl von Ossietzky Universität Oldenburg (BIS), Odenburg, Germany, pp. 97–105.

Shields-Zhou, G., Och, L., 2011. The case for a neoproterozoic oxygenation event: geochemical evidence and biological consequences. GSA Today 21, 4–11. https://doi.org/10.1130/GSATG102A.1.

Slotznick, S.P., Sperling, E.A., Tosca, N.J., Miller, A.J., Clayton, K.E., van Helmond, N.A.G.M., Slomp, C.P., Swanson-Hysell, N.L., 2020. Unraveling the mineralogical complexity of sediment iron speciation using sequential extractions. Geochem. Geophys. Geosyst. 21. https://doi.org/10.1029/2019GC008666.

Spangenberg, J.E., Bagnoud-Velásquez, M., Boggiani, P.C., Gaucher, C., 2014. Redox variations and bioproductivity in the Ediacaran: Evidence from inorganic and organic geochemistry of the Corumbá Group, Brazil. Gondwana Res. 26, 1186–1207. https://doi.org/10.1016/j.gr.2013.08.014.

Sperling, E.A., Frieder, C.A., Raman, A.V., Girguis, P.R., Levin, L.A., Knoll, A.H., 2013. Oxygen, ecology, and the Cambrian radiation of animals. Proc. Natl. Acad. Sci. 110, 13446–13451. https://doi.org/10.1073/pnas.1312778110.

Sperling, E.A., Wolock, C.J., Morgan, A.S., Gill, B.C., Kunzmann, M., Halverson, G.P., Macdonald, F.A., Knoll, A.H., Johnston, D.T., 2015. Statistical analysis of iron geochemical data suggests limited late Proterozoic oxygenation. Nature 523, 451–454. https://doi.org/10.1038/nature14589.

Sperling, E.A., Melchin, M.J., Fraser, T., Stockey, R.G., Farrell, U.C., Bhajan, L., Brunoir, T.N., Cole, D.B., Gill, B.C., Lenz, A., Loydell, D.K., Malinowski, J., Miller, A.J., Plaza-Torres, S., Bock, B., Rooney, A.D., Tecklenburg, S.A., Vogel, J.M., Planavsky, N.J., Strauss, J.V., 2021. A long-term record of early to mid-Paleozoic marine redox change. Sci. Adv. 7. https://doi.org/10.1126/SCIADV.ABF4382.

Sperling, E.A., Boag, T.H., Duncan, M.I., Endriga, C.R., Marquez, J.A., Mills, D.B., Monarrez, P.M., Sclafani, J.A., Stockey, R.G., Payne, J.L., 2022. Breathless through time: oxygen and animals across earth's history. Biol. Bull. 243, 184–206. https://doi.org/10.1086/721754.

Squire, R.J., Campbell, I.H., Allen, C.M., Wilson, C.J.L., 2006. Did the Transgondwanan Supermountain trigger the explosive radiation of animals on Earth? Earth Planet. Sci. Lett. 250, 116–133. https://doi.org/10.1016/j.epsl.2006.07.032.

Stockey, R., Pohl, A., Ridgwell, A., Finnegan, S., Sperling, E.A., 2021. Decreasing phanerozoic extinction intensity is a predictable consequence of earth surface oxygenation and metazoan ecophysiology. Proc. Natl. Acad. Sci. 118, e2101900118. https://doi.org/10.1073/pnas.2101900118.

Stookey, L.L., 1970. Ferrozine - a new spectrophotometric reagent for iron. Anal. Chem. 42, 779–781.

Tarhan, L.G., Zhao, M., Planavsky, N.J., 2021. Bioturbation feedbacks on the phosphorus cycle. Earth Planet. Sci. Lett. 566, 116961. https://doi.org/10.1016/J.EPSL.2021.116961.

Tohver, E., Trindade, R.I.F.I.F., Solum, J.G.G., Hall, C.M.M., Riccomini, C., Nogueira, A.C.C., 2010. Closing the Clymene ocean and bending a Brasiliano belt: Evidence for the Cambrian formation of Gondwana, southeast Amazon craton. Geology 38, 267–270. https://doi.org/10.1130/G30510.1.

Tostevin, R., Mills, B.W., 2020. Reconciling proxy records and models of Earth's oxygenation during the Neoproterozoic and Palaeozoic: Neoproterozoic-Palaeozoic Oxygenation. Interface Focus 10. https://doi.org/10.1098/rsfs.2019.0137rsfs20190137.

Tostevin, R., Wood, R.A., Shields, G.A., Poulton, S.W., Guilbaud, R., Bowyer, F., Penny, A.M., He, T., Curtis, A., Hoffmann, K.H., Clarkson, M.O., 2016. Low-oxygen waters limited habitable space for early animals. Nat. Commun. 7, 1–9. https://doi.org/10.1038/ncomms12818.

Trompette, R., de Alvarenga, C.J.S., Walde, D., 1998. Geological evolution of the Neoproterozoic Corumbágraben system (Brazil). Depositional context of the stratified Fe and Mn ores of the Jacadigo Group. J. South Am. Earth Sci. 11, 587–597. https://doi.org/10.1016/S0895-9811(98)00036-4.

Walde, D.H.G., Do Carmo, D.A., Guimarães, E.M., Vieira, L.C., Erdtmann, B.D., Sanchez, E.A.M., Adorno, R.R., Tobias, T.C., 2015. New aspects of Neoproterozoic-Cambrian transition in the Corumbá region (state of Mato Grosso do Sul, Brazil). Ann. Paleontol. 101, 213–224. https://doi.org/10.1016/j.annpal.2015.07.002.

Wei, G.Y., Planavsky, N.J., Tarhan, L.G., Chen, X., Wei, W., Li, D., Ling, H.F., 2018. Marine redox fluctuation as a potential trigger for the Cambrian explosion. Geology 46, 587–590. https://doi.org/10.1130/G40150.1.

Wood, R., Liu, A.G., Bowyer, F., Wilby, P.R., Dunn, F.S., Kenchington, C.G., Cuthill, J.F.H., Mitchell, E.G., Penny, A., 2019. Integrated records of environmental change and evolution challenge the Cambrian Explosion. Nat. Ecol. Evol. 3, 528–538. https://doi.org/10.1038/s41559-019-0821-6.

Wood, R.A., Poulton, S.W., Prave, A.R., Hoffmann, K.H., Clarkson, M.O., Guilbaud, R., Lyne, J.W., Tostevin, R., Bowyer, F., Penny, A.M., Curtis, A., Kasemann, S.A., 2015. Dynamic redox conditions control late Ediacaran metazoan ecosystems in the Nama Group, Namibia. Precambrian Res. 261, 252–271. https://doi.org/10.1016/j.precamres.2015.02.004.

Xiao, S., Laflamme, M., 2009. On the eve of animal radiation: phylogeny, ecology and evolution of the Ediacara biota. Trends Ecol. Evol. 24, 31–40. https://doi.org/10.1016/j.tree.2008.07.015.

Zaine, M., 1991. Análise dos fósseis de parte da Faixa Paraguai (MS, MT) e seu contexto temporal e paleoambiental. Universidade de São Paulo (in Spanish).